Coding Metasurfaces with Reconfiguration Capabilities Based on Optical Activation of Phase-Change Materials for Terahertz Beam Manipulations

Quan-wei Lin, Hang Wong, Laure Huitema, Aurelian Crunteanu

Coding Metasurfaces with Reconfiguration Capabilities Based on Optical Activation of Phase Change Materials for Terahertz Beam Manipulations

Quan-Wei Lin, Hang Wong, Laure Huitema, and Aurelian Crunteanu*

Dr. Quan-Wei Lin, Dr. Hang Wong
State Key Laboratory of Terahertz and Millimeter Waves, City University of Hong Kong, Hong Kong SAR, China
E-mail: hang.wong@cityu.edu.hk

Dr. Laure Huitema, Dr. Aurelian Crunteanu
XLIM Research Institute, CNRS/ University of Limoges, Limoges 87060, France

Keywords: terahertz, metasurface, coding, phase-change material, beam manipulation

Abstract: Ultrafast reconfigurable devices with high-speed responses, high-resolution capabilities and ultra-compact sizes will be essential for future real-time terahertz imaging, chemical detection, nondestructive biosensing and communication systems. Multifunctional terahertz metasurfaces with active, programmable controls have enabled conspicuous functionalities of subwavelength planar devices and components for manipulating electromagnetic (EM) waves such as beam focusing, polarization modification, generation of exotic EM modes or multibeam scanning applications. However, active metasurface technologies for EM beam manipulation, capable of dynamical topology change or induced-phase reconfiguration, are usually requiring various semiconductor-based controlling elements (e.g. PN diodes, transistors) which are difficult to implement in the high frequency spectrum of terahertz waves. In this work, we introduce a coding metasurface integrating patterned GeTe phase change materials as command elements, which allows the optical control of terahertz wave propagation. The suggested metasurface design brings plentiful of remarkable functionalities through different coding patterns and is highly effective to control beam tilting, directivity, and splitting of terahertz beams. The proposed concepts of coding metasurfaces integrating optically active phase change materials were successfully confirmed by experimental demonstration and could be extended to more complex terahertz systems for imaging, tomography, sensing, and 6G communication applications.

1. Introduction

Terahertz metadevices have rich functionalities in providing light and wave manipulations for different areas of applications.[1] These classes of high-frequency devices are able to control the propagation of electromagnetic (EM) waves for specific purposes such as re-distribution of the EM wavefronts,[2] conversion of the wave polarization,[3] and manipulation of reflected or transmitted radiating beam direction.[4] Technological developments in this field have resulted in the emergence of demonstrators at terahertz frequencies such as polarizers,[5] switches,[6] sensors,[7] and beam controllers[8] having high-efficiency and fast-response performance. Many studies of EM wave control have validated the ability of metadevices to broaden the operating bandwidth,[3a, 9] enhance the radiation efficiency[10] and get rid of aberrations related to amplitude and phase distortions in wave propagations.[3a, 9] However, most of the designs associated with these demonstrations are passive metasurfaces that are bounded by their single functionality related to their fixed structures and limited to binary states modulation and restricted switching speed. To date, several approaches have been introduced to realize active metasurfaces whose planar structures could be dynamically reconfigured by external stimuli[2b, 3a, 11] and thus, providing multifunctional features to metadevices. This dynamic modification of the metasurfaces topologies,[12] presenting extended levels of wave manipulation, can be provided by the integration of semiconductors,[13] 2D materials,[14] super conductors,[15] liquid metal,[16] photodiodes[17] and phase-change materials[18] like VO_2, [19] and $Ge_2Sb_2Te_5$ (GST).[13d, 20] All of these active control methods have shown remarkable capabilities in modulating the responses of metadevices through thermal, optical, or electrical stimuli, with their own respective edges. Thanks to the ultrafast responses of semiconductors (diodes or varactor diodes) on the meta atom in the metasurface,[13] real-time reconfigurability of polarization and radiation direction can be realized. However, p-n junction diode shows low efficiency in terahertz frequency region, which limits its application in microwave band. Among these

approaches, chalcogenide phase change materials with their ability of reversible conversion between two stable amorphous (insulator) and crystalline (conductive) binary states are the most ideal platform for the realization of multifunctional terahertz metadevices due to their ultrafast phase change response, easy fabrication, semiconductor-compatibility integration, broadband responses and, especially, nonvolatility with zero hold power. Although in recent years, many excellent demonstrations for modulating terahertz waves using metasurfaces arose, there was no experimental evidence shown available active metasurfaces integrating phase change materials that could be able to manipulate wave propagation at terahertz frequencies.

Phase change material GST has been successfully integrated for optically controllable coding metasurfaces and photonic devices,[11b] being successful in demonstrating variable focus and multi-focus planar Fresnel-zone plates or dynamically reconfigurable dielectric metamaterials with non-volatile properties in the infrared (IR) domain. Recently, the GST and GeTe compositions were also evaluated towards their response in the terahertz domain with demonstrations of efficient manipulation of terahertz waves through their integration in split-ring resonators-based metamaterials[18d] or incorporation of multilevel nonvolatile resonant states of metamaterial structures.[21] These incipient demonstrations in the terahertz domain exploit the thermal- or electrical-induced phase change of phase-change materials which are effective to transform the material from the amorphous to its crystalline state but less operational to perform the reverse transition on large-scale areas. In contrast, the optical-induced activation of phase change materials between their dissimilar states with contrasting optical and electrical properties has been successfully proven for large-areas devices operating in the optical,[11b] microwaves[22] or terahertz domains.[23]

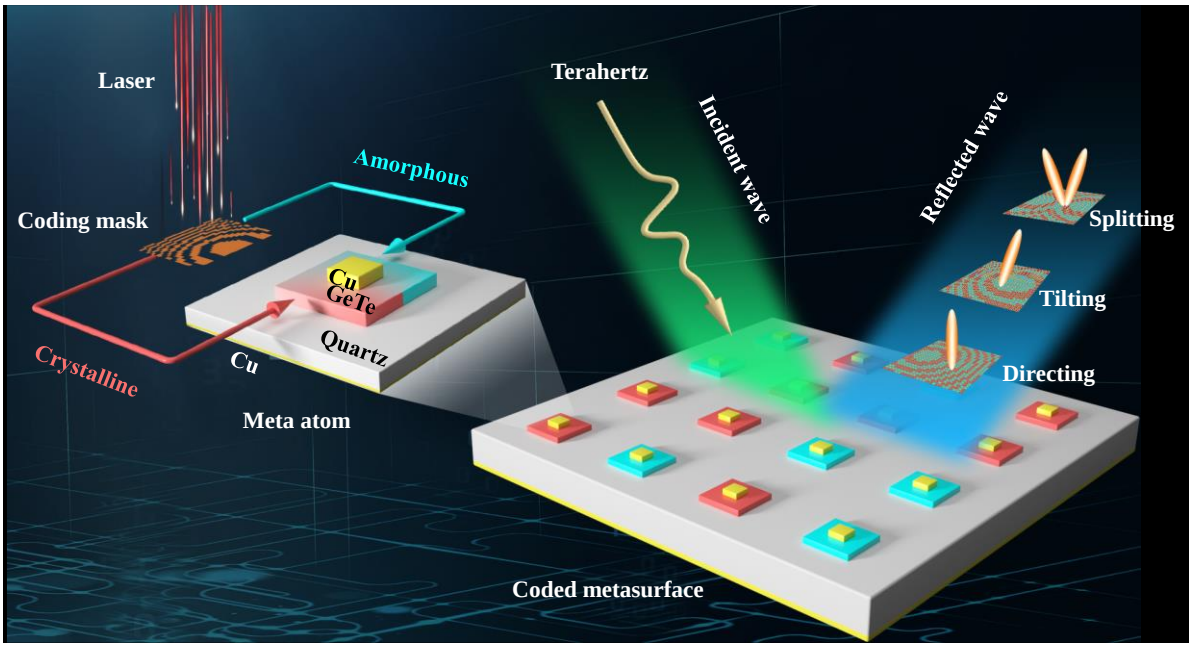

Figure 1. Schematic illustration of the proposed optical-based coding metasurface for multifunctional control of terahertz beam: The coding metasurface is composed of meta-atoms based on *GeTe* phase change material. Through selective laser activation using a properly designed coding mask, the specific states of each *GeTe*-based meta-atom can be switched between crystalline (conductive) and amorphous (insulating) phases, allowing the metasurface to perform multifunctional control of terahertz waves including beam splitting, beam tilting, and beam focusing.

In this paper, we are reporting for the first time the experimental demonstration of optical-based coding metasurface for multifunctional control of terahertz waves. The proposed coding metasurface is based on large array of hybrid meta-atoms integrating the phase change GeTe material. The simple structure of the meta-atom – hybrid integration of metal and GeTe patterns on a silica substrate, provides the effective modification of an incident wave phase by the optical control of the GeTe material specific state. This characteristic allows for constructing the spatial coding of the meta-atoms array with different combinations of meta-atoms through optical irradiation, which offers to the proposed metasuface powerful capabilities in controlling the terahertz wave propagation. In order to validate the proposed concept, we fabricated five metasurfaces with different coding patterns prepared through UV-laser irradiation of the integrated GeTe patterns through contact masks corresponding to a specific coding functionality. Moreover, we experimentally demonstrate that the coding metasurface is capable

of manipulating the terahertz wave for beam tilting, directing, and splitting. We envision that this new proposed approach of designing and controlling metasurfaces at terahertz frequencies might be an effective tool for future integration in terahertz systems for imaging/ tomography, sensing, and 6G communication applications.

2. Results and discussion

2.1. Design of the Coding Metamaterial Atoms

The reconfiguration of coded patterns on the metasurface is realized by the optical control of the individual states of its constituent meta-atoms. It allows producing the desirable reflected waves with specific functions. The operating principle of the terahertz metasurface is schematically represented in **Figure 1**. The metadevice is composed of meta-atoms based on *GeTe* functional material. Through selective laser activation using a properly designed coding mask, the specific states of the *GeTe* layers on meta-atoms can be configured between crystalline (conductive) and amorphous (insulating) states, allowing the specifically patterned metasurface to perform multifunctional control of terahertz waves. The coding mask determines the distribution of the crystalline pattern of the *GeTe*-based meta-atoms on the metasurface. When an incident wave is propagating to the metasurface, the reflected wave can be manipulated by controlling the encoded pattern on it and results in different and particular types of reflected radiation beams.

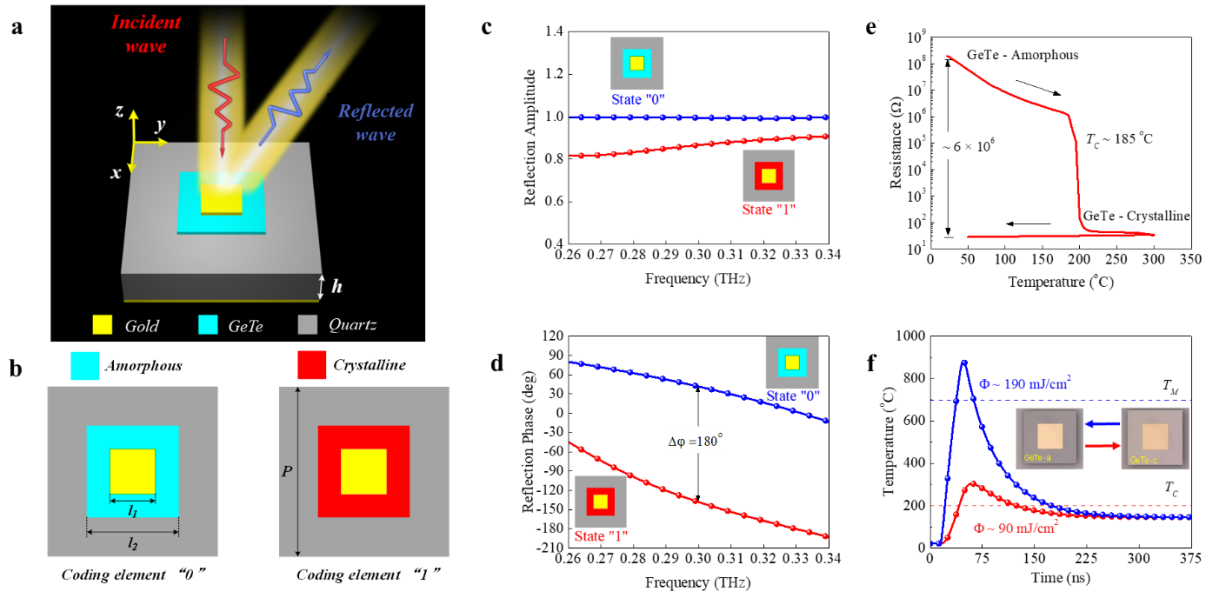

Figure 2. Design and properties of the proposed optically controlled coding element. a) The detailed structure of the meta atom coding element with a 1-μm thick gold squares on top of a 1-μm thick *GeTe* squared patterns build on a SiO_2 substrates. **b)** Schematics of two states of the coding element: state "0" indicates the amorphous (insulating) state of *GeTe*, state "1" indicates the crystalline (conductive) state of *GeTe*. **c)** and **d)** The corresponding reflection properties (c- amplitude and d- phase) of the coding element in the two states. **e)** Temperature-dependent variation of the surface resistance of a *GeTe* layer (2-probe measurement) displaying more than six orders of difference in electrical properties between the two states and the non-volatile behavior of the crystalline state upon cooling to room temperature. **f)** Finite-elements simulations of the temperature rise of the *GeTe* layer upon 35-ns long single-pulse UV laser irradiation having dissimilar energy densities: a single pulse having fluencies of 90 mJ/cm^2 will rise the temperature of the initially-amorphous *GeTe* above its crystallization temperature (T_C), while a subsequent 190-mJ/cm^2 laser pulse will heat the *GeTe* above its local melting temperature T_M and will melt-quench the material back to the amorphous state.

A closer look of the configuration and schematic of the proposed 1-bit meta-atom is depicted in **Figure 2a**. The relative permittivity and conductivity of the amorphous *GeTe* are 63 and 10 S/m, while those of the crystalline *GeTe* are 1 and 410000 S/m. Thus, depending on the particular state of the *GeTe* functional material (amorphous/insulator or crystalline/ conductive), the meta-atom can be seen as a two-state coding element: "0"- for the *GeTe* in the amorphous phase and "1"- for *GeTe* in the crystalline state (Figure 2b). In particular, the dimensions and design of the meta-atom are chosen for providing distinct responses for the "0" and "1" states (reflected amplitude and phase) to an incident terahertz wave (Figure 2c and Figure 2d), especially for obtaining opposite coding states with 180° (π) phase difference at 0.3

THz. In this meta-atom design, a small square metal patch is placed on top of the *GeTe* material for improving the reflection efficiency in the large array of meta-atoms of the proposed coding metasurface. Although the reflection amplitude of state "1" is lower than that of state "0" this can be further improved by increasing the thickness of the GeTe pattern (Figure S1, Supporting Information). Details on the influence of the *GeTe* material electrical parameters on the performance of the coding elements in both states are given in the supporting information and associated Figures S2 and S3.

Thus, the array of hybrid meta-atoms is based on 229 μm × 229 μm *GeTe* square-shaped patterns having a thickness of 1 μm and fabricated on a 100-μm thick quartz substrate (ε_r = 3.8). On top of each *GeTe* patterns are placed 107 μm × 107 μm metal patches made by titanium/ gold bilayer (Ti/ Au – 40/ 1000 nm). A 1-μm thick metal Ti/ Au bilayer is fabricated beneath the quartz layer and is acting as the metasurface ground plane.

The *GeTe* layer integrating the meta-atoms is showing more than six orders of magnitude change (Figure 2e) in electrical properties (DC resistance) between its amorphous (insulating) and its crystalline (conductive) states and a transition temperature to the crystalline state situated around 185°C. It may be noticed that the material retains its conductive behavior (non-volatility of states) upon cooling back to the room temperature. The thermal transformation of the material from the crystalline phase back to its amorphous one implies a rapid melt-quenching process and occurs through the destruction of the crystalline order in the material (local melting) and the fast cooling of this state towards a disordered, amorphous phase.[24] This melt-quench process, essential to the reversible phase transitions in phase change materials can be achieved with short electrical or laser pulses.[25] In our experiments, we are performing irradiation of the *GeTe* material using single laser pulses from a large-area beam of a *KrF* excimer laser operating at 248 nm and having pulse lengths of ~ 35 ns with on-demand optical energies. The finite-elements simulations using Comsol Multiphysics of laser-beam-GeTe material interactions (Figure 2f) show that a single laser pulse with an energy density of 90

mJ/cm^2 will rise the temperature of the initially-amorphous *GeTe* layer above its crystallization temperature T_C and will transform the material to its conducting state. Conversely, a subsequent 190-mJ/cm^2 laser pulse will bring the now-crystalline *GeTe* material above its local melting temperature T_M and will quench it back to the amorphous state on a fast timescale which will prevent its re-crystallization.

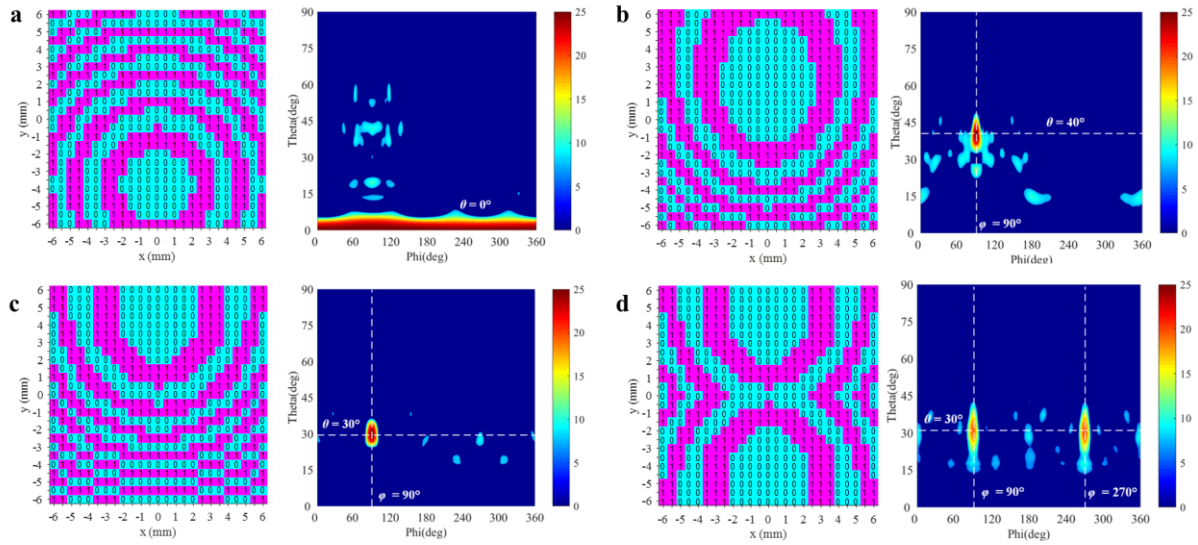

Figure 3. The designed coding patterns and the simulated far-field results of the coding metasurface for different feeding angles (θ_{in}) of the incident EM waves, resulting in specific reflection beam angles (θ_{rad}), as a function of the coded pattern. a) Optically coded function 1 (reflection beam angle of 0° with feeding antenna locating at azimuth angle of 30°). **b)** Optically coded function 2 (reflection beam angle of 40° with feeding antenna locating at azimuth angle of 30°). **c)** Optically coded function 3 (reflection beam angle of 30° with feeding antenna locating at azimuth angle of 0°). **d)** Optically coded function 4 (dual beam radiations reflected at ± 30° with feeding antenna locating at azimuth angle of 0°).

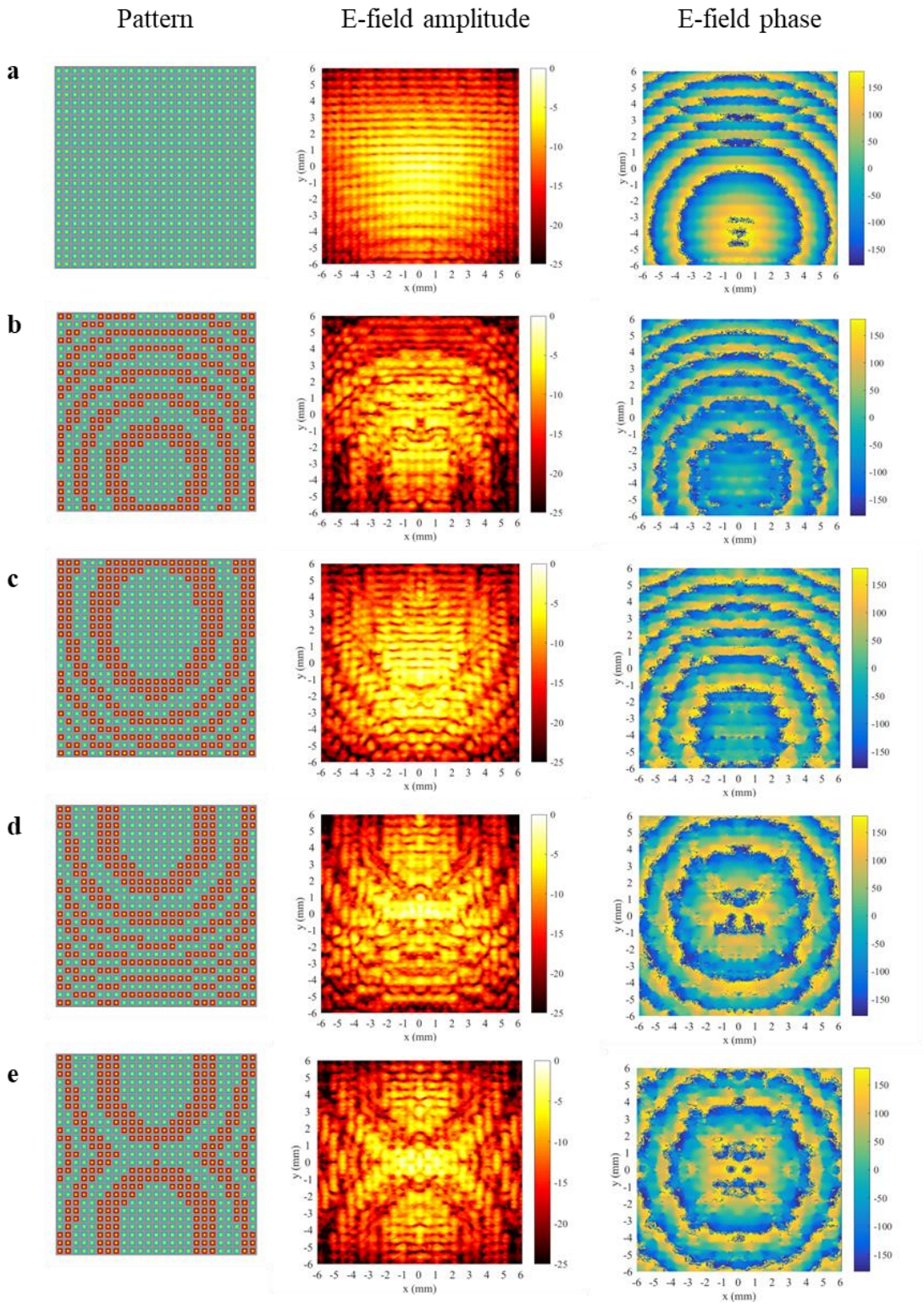

Figure 4. Simulation models and E-field distributions (amplitude and phase) of the coding metasurface for EM waves at different incident angles (θ_{in}) and maximum reflection beam angles (θ_{rad}). a) Metasurface without coding pattern. **b)** Coding metasurface for reflection beam angle of 0° with feeding antenna locating at azimuth angle of 30°. **c)** Coding metasurface for reflection beam angle of 40° with feeding antenna locating at azimuth angle of 30°. **d)** Coding metasurface for reflection beam angle of 30 ° with feeding antenna locating at azimuth angle of 0°. **e)** Coding metasurface for dual beam radiations reflected at ± 30° with feeding antenna locating at azimuth angle of 0°.

2.2. Design of Coding Metasurface

The coding metasurface design is meant to manipulate the direction beam of a reflected terahertz wave with different angles. As mentioned above, this control of the beam direction is determined by a 2D planar array of meta-atoms with dissimilar states of the metasurface. Confirmed from the results shown on Figure 2d, the proposed meta-atom has stable reflection loss and 180° (π) phase difference between amorphous and crystalline states. This individual characteristic of meta-atoms allows compensating the phases of the reflected wave in order to generate highly efficient directed beams. The required compensated phase for every single atom is determined by $\varphi_e = k_0\left(\left|\vec{r}_e - \vec{r}_f\right| - F - \hat{u}\vec{r}_e\right)$, where k_0 is the free-space wavenumber and $\vec{r}_e = (x_e, y_e, 0)$ is the position vector of the atom, $\vec{r}_f$ is the position vector of the feeding antenna, F is the distance between the incident feeding source and the center of metasurface, is the vector of the reflected main beam direction.[26] Therefore, for desired phases that are 131.5° ≤ φ_e < 311.5°, the *GeTe* film of meta-atom must be in the crystalline state which is represented as State "1". On the other hand, for desired phases that are 0 ≤ φ_e < 131.5° and 311.5° ≤ φ_e < 360°, the *GeTe* film of meta-atom should be in the amorphous state which is represented as State "0". The resulted coding patterns for different incident angles of feeding antenna and different desired reflected angles are presented in **Figure 3**. The proposed metasurface is composed by 25 × 25 meta-atoms which is suitable to shape the radiation beam emitted from the feeding source.

We simulated the designed metasurfaces shown in Figure 3 integrated with feeding antenna by using the high-frequency EM simulator HFSS. The simulation of the coding metasurfaces with different coding patterns (**Figure 4**) shows that the reflected electric field distribution on the top surface of the metasurface can be controlled by the coding pattern on the metasurface, so that the reflected terahertz wave can be manipulated and produced at different angles. In the metasurface pattern configurations shown on Figure 4, green pads represent the meta atoms in

State “0” (with GeTe pattern in amorphous state) while red ones represent the meta atoms in crystalline State “1” (with GeTe pattern in crystalline state).

The electric field distribution in the case where all atoms are in the amorphous state (Figure 4a) is a reference for comparisons with different following cases (Figure 4b to Figure 4e). An antenna source is located at a distance of 7.72 mm at an incident angle of 30° (θ_{in} = 30°) to the metasurface. From the simulated result in Figure 4a, amplitudes and phases of the reflected electric field could not produce a focusing beam. This distribution of the electric field (Figure 4a) is typical to a reflection from a pure reflector only. When the pattern of the metasurface is coded as shown in Figure 4b and Figure 4c, the electric field distributions are modified to direct the reflected beam of the incident wave (same as the reference θ_{in} = 30°), to θ_{rad} = 0° and 40° respectively. On the other hand, the metasurface can also operate under different angles of the incident wave. Thus, in the example shown in Figure 4d, the antenna source is placed at a distance of 7.72 mm with an incident angle of 0° to the metasurface. The coded pattern of the metasurface can be reconfigured to re-arrange the surface electric field distribution and generate the reflected wave to the direction of θ_{rad} = 30°. Furthermore, the proposed metasurface can be used for generating beam splitting through the control of the coded pattern on the metasurface which can form a mirror-type electric field distribution (Figure 4e), such that two identical reflected beams can be delivered to the direction of θ_{rad} = ± 30° from the incident wave (θ_{in} = 0°).

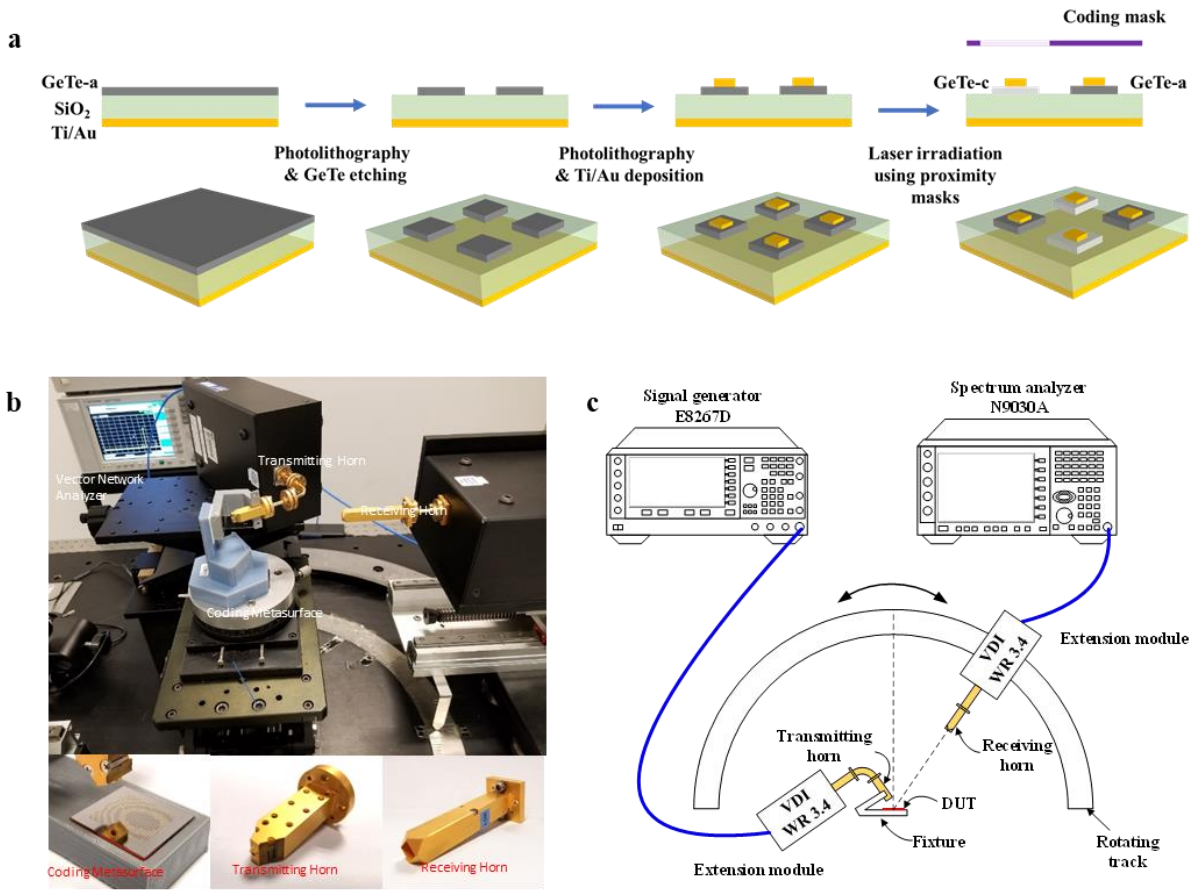

Figure 5 Realization and measurement setup of the coded metadevice performing beam manipulation. a) Cross-section and 3D-view schematics of sample fabrication process. **b)** Experimental setup for different beam angle device excitation and measurement using far-field scanning technique. **c)** Platform for the far-field measurement of radiation patterns.

To validate the performance of the proposed design and reconfiguration methodology, we fabricated the prototypes of the coded metasurface with the five coded patterns shown in Figure 4a-e and measured their performances by setting up a THz far-field measurement platform as shown in **Figure 5 (**additional information on the measurement scheme is given in the supporting information associated with Figure S4**)**. The as-fabricated device is corresponding to the metasurface depicted in **Figure 6a** for which all *GeTe* patterns are in the amorphous state (all the meta-atoms in State "0"). The coding pattern describing a particular coding function of the coding metasurface (specific distribution of amorphous and crystalline *GeTe* patterns) was imprinted by laser irradiation of the *GeTe* patterns through a proximity contact mask whose design is related to a specific metadevice function. Using dissimilar laser writing/ erasing

energies (as described in **Figure 2f**), the *GeTe* integrating a meta-atom can be transformed between the two amorphous and crystalline states, with a spatial distribution corresponding to the desired coding pattern.

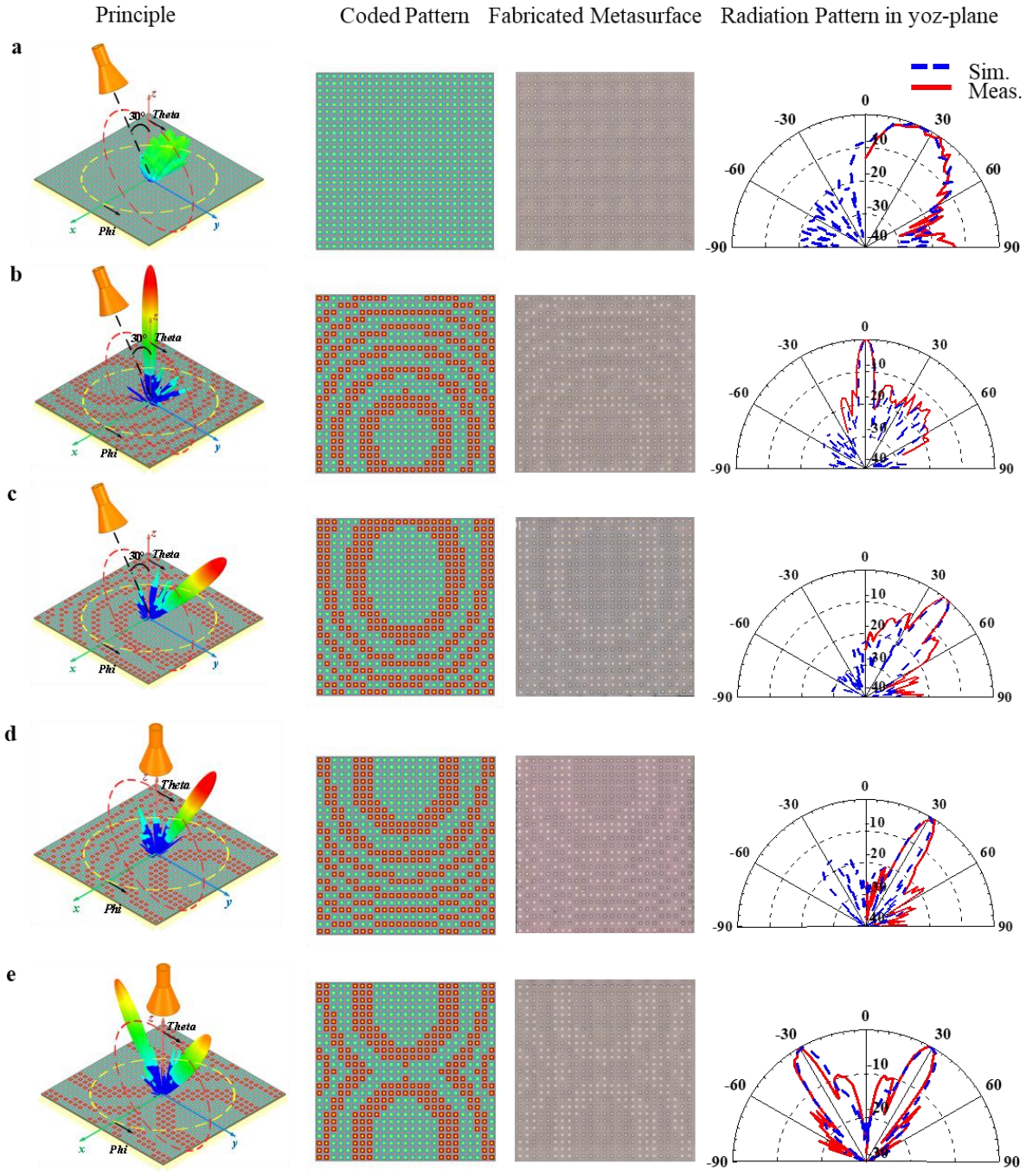

Figure 6. Simulated and experimental results of the proposed coding metasurface used to control the reflected beam parameters of incident EM waves. Here are presented for each row, from left to right: the schematic set-up of the metasurface excitation by a horn antenna and the 3D-simulated reflected radiation diagram, the specific pattern of the coding metasurface,

the fabricated metasurface corresponding to the coded pattern, and the comparisons between the simulated (blue dotted curves) and measured (red curves) results of the normalized far-field diagrams of the reflected EM waves. **a)** Optically coded function 0 (uncoded metasurface)**. b)** Optically coded function 1 (reflection beam angle of 0° with feeding antenna locating at azimuth angle of 30°). **c)** Optically coded function 2 (reflection beam angle of 40° with feeding antenna locating at azimuth angle of 30°). **d)** Optically coded function 3 (reflection beam angle of 30 ° with feeding antenna locating at azimuth angle of 0°). **e)** Optically coded function 4 (dual beam radiations reflected at ± 30° with feeding antenna locating at azimuth angle of 0°).

Figure 6 illustrates the simulated and measured results of the radiation patterns of different terahertz encoded functions for the each specific coding metasurface. The electromagnetic simulation of the excitation [A1]scheme, the associated coded pattern, the fabricated prototype and the experimental measurement of the radiation patterns in yoz-plane are represented from left to right for different coding states corresponding to each row. Figure 6a shows the results for the case where the *GeTe* patterns in the metasurface are all in the amorphous states (all meta-atoms in State "0"). It can be found that the metasurface in this state cannot focus the incident wave but only reflects it at φ=90°, θ_{rad}=30°. By placing a coding mask on top of this metasurface and performing laser irradiation of particular *GeTe*-based meta-atoms, the required phases of meta-atoms that should be opposite to the phase center can be altered to π by changing specific *GeTe* patterns into their crystalline state (State "1" of the meta-atoms). The optical activation of *GeTe* through specific coding masks allows to obtain the desired coding functions of the metasurface which may be used to reflect the incident terahertz waves at different angles. The measured results of the radiation patterns for all the investigated coded functions show excellent agreement with the simulated ones.

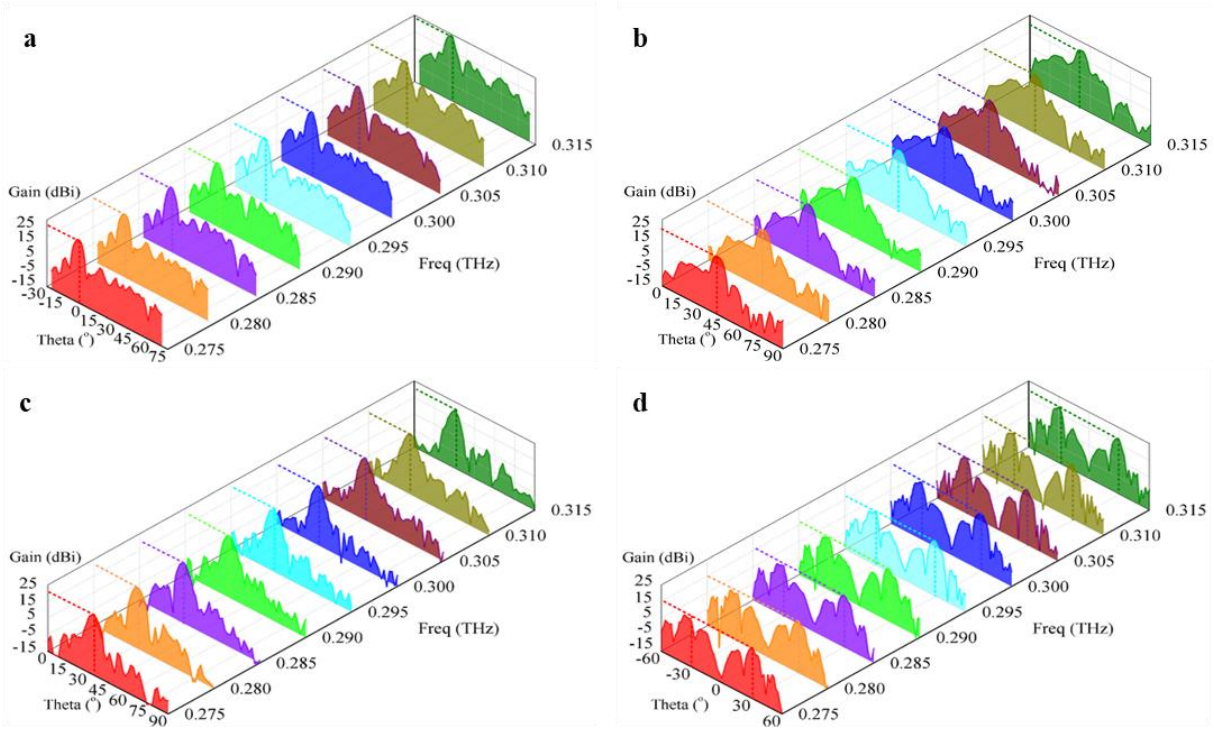

Figure 7. Experimental radiation gain results of the reflected EM waves for different coded function configurations as a function of EM radiation frequencies ranging from 0.275 THz to 0.315 THz. a) Reflection beam angle at 0° with feeding antenna locating at azimuth angle of 30° (coded function 1). **b)** Reflection beam angle at 40° with feeding antenna locating at azimuth angle of 30° (coded function 2). **c)** Reflection beam angle of 30° with feeding antenna locating at azimuth angle of 0° (coded function 3). **d)** Dual beam reflected radiation at ± 30° with feeding antenna locating at azimuth angle of 0° (coded function 4).

Such a high-efficient phase controlling methodology enables to manipulate an incident terahertz beam within a wide bandwidth, as illustrated in **Figure 7**. The maximum measured reflected beam angle at coded function 1 varies from -3° to +2° for frequencies ranging from 0.275 THz to 0.315 THz while the maximum measured reflected beam angle at coded function 2 varies from +38° to +42°. Similarly, the maximum measured reflected beam angle at coded function 3 varies from +30° to +34° and the two maximum reflected beam angles of coded function 4 varies from +28° to +32° and -34° to -30°. Thus, the resulted radiation patterns and associated

gains are stable within the investigated bandwidth. These experimental results validate the powerful capability of the proposed design in transforming the metasurface functionality through coding pattern reconfiguration.

3. Conclusion

We designed and experimentally demonstrated terahertz wave beamforming using an original approach based on optical activation of *GeTe* material integrating the constituent meta-atoms of a coding metasurface. The simple structure of the meta-atom – based on hybrid integration of metal and *GeTe* patterns on a silica substrate, allows the effective modification of an incident wave phase by optical control of the specific state of the *GeTe* material and is highly effective in controlling the propagation of incident wave over wide terahertz frequency domains. Moreover, the capability of the proposed coding metasurface in manipulating the terahertz wave for beam tilting, directing, and splitting is verified by the experiment while the measured results show excellent agreement with the simulated ones . Besides validating the integration of phase change materials in terahertz coding metasurface, the novel proposed methodology can be further expanded towards real-time, on-demand, optically prepared terahertz functions using raster or sequential optical scanning and the writing/ erasing capabilities of phase change materials integrating such metasurfaces. We foresee that this new proposed approach of designing and controlling metadevices at terahertz frequencies can find potential applications in terahertz devices and systems for imaging/ tomography, sensing, and 6G communication applications.

4. Experimental Section

4.1 Device simulation[A2]

4.2. Prototype Fabrication

The coding metasurface was fabricated following the steps schematically represented in Figure 5a. A 1-μm thick metallic ground layer (*Au*/*Ti* by electron-beam evaporation) is firstly deposited on a 100-μm thick quartz wafer followed by *GeTe* layer deposition on the opposing substrate side (1-μm thick GeTe layer using DC magnetron sputtering from a high-purity 50-50 Ge-Te target). It follows two photolithographic steps allowing defining the *GeTe* patterns and the electron-beam deposition of the Au/Ti (1000-40 nm) metallic patches on top of GeTe.

4.3. Measurement

The performances of the fabricated prototypes were evaluated using an in-house designed far-field terahertz measurement platform shown in Figure 5b-c. The platform is composed of a signal generator, a spectrum analyzer, two millimeter-wave signal generator extension modules, a feeding horn antenna and a receiving horn antenna. The under-test metasurface is placed at the center of a semi-circle rotating track. The device is mounted on a 3D-printed fixture allowing to precisely adjust the specific incident angle between the feeding antenna and the metadevice. An extension module (VDI WR 3.4) is adapted to expand the measurement frequency range of the signal generator (Agilent E8267D) to WR-3.4 (0.22 THz-0.33 THz domain). A +10 dBm signal (frequency ranging from 18.3 – 27.5 GHz) fed by the signal generator is multiplied in the extension module to a millimeter wave signal at 0.22 THz-0.33 THz. The output millimeter wave signal is reduced to -2 dBm (typical) and enters the transmitting horn antenna. An additional extension module accommodating the receiving horn antenna is placed on the rotating track to detect the reflected radiating signal from the device. The typical dynamic range for the receiving power is 115 dB which is adequate for the signal detection.

Acknowledgements
This work was supported in part by the Research Grants Council of the Hong Kong SAR, China (Project No. CityU 11218318 and CRF CityU C1020-19E).

References

[1] a) N. I. Zheludev, Y. S. Kivshar, *Nature materials* **2012**, 11, 917; b) L. Liu, L. Kang, T. S. Mayer, D. H. Werner, *Nature communications* **2016**, 7, 1.

[2] a) T. J. Cui, M. Q. Qi, X. Wan, J. Zhao, Q. Cheng, *Light: Science & Applications* **2014**, 3, e218; b) Y.-W. Huang, H. W. H. Lee, R. Sokhoyan, R. A. Pala, K. Thyagarajan, S. Han, D. P. Tsai, H. A. Atwater, *Nano letters* **2016**, 16, 5319; c) L. Zhang, X. Q. Chen, S. Liu, Q. Zhang, J. Zhao, J. Y. Dai, G. D. Bai, X. Wan, Q. Cheng, G. Castaldi, *Nature communications* **2018**, 9, 1; d) L. Zhang, X. Q. Chen, R. W. Shao, J. Y. Dai, Q. Cheng, G. Castaldi, V. Galdi, T. J. Cui, *Advanced Materials* **2019**, 31, 1904069.

[3] a) Z. Miao, Q. Wu, X. Li, Q. He, K. Ding, Z. An, Y. Zhang, L. Zhou, *Physical Review X* **2015**, 5, 041027; b) P. Li, X. Yang, T. W. Maß, J. Hanss, M. Lewin, A.-K. U. Michel, M. Wuttig, T. Taubner, *Nature materials* **2016**, 15, 870; c) R. Drevinskas, M. Beresna, J. Zhang, A. G. Kazanskii, P. G. Kazansky, *Advanced Optical Materials* **2017**, 5, 1600575; d) L. Cong, Y. K. Srivastava, H. Zhang, X. Zhang, J. Han, R. Singh, *Light: Science & Applications* **2018**, 7, 1.

[4] a) A. Arbabi, E. Arbabi, Y. Horie, S. M. Kamali, A. Faraon, *Nature Photonics* **2017**, 11, 415; b) L. Zhang, R. Y. Wu, G. D. Bai, H. T. Wu, Q. Ma, X. Q. Chen, T. J. Cui, *Advanced Functional Materials* **2018**, 28, 1802205; c) Q. Ma, G. D. Bai, H. B. Jing, C. Yang, L. Li, T. J. Cui, *Light: Science & Applications* **2019**, 8, 1.

[5] a) J.-H. Shin, K. Moon, E. S. Lee, I.-M. Lee, K. H. Park, *Nanotechnology* **2015**, 26, 315203; b) Y. Zhao, A. Qing, Y. Meng, Z. Song, C. Lin, *Scientific reports* **2018**, 8, 1.

[6] a) N. El-Hinnawy, P. Borodulin, E. B. Jones, B. P. Wagner, M. R. King, J. S. Mason, J. Hartman, R. Howell, M. Lee, R. Young, presented at CS MANTECH Conf. **2014**; b) W. Vitale, M. Tamagnone, N. Émond, B. Le Drogoff, S. Capdevila, A. Skrivervik, M. Chaker, J. Mosig, A. Ionescu, *Scientific reports* **2017**, 7, 1.

[7] a) J. Fang, I. Levchenko, W. Yan, I. Aharonovich, M. Aramesh, S. Prawer, K. Ostrikov, *Advanced Optical Materials* **2015**, 3, 750; b) W. Wang, F. Yan, S. Tan, H. Zhou, Y. Hou, *Photonics Research* **2017**, 5, 571.

[8] a) M. Khorasaninejad, W. Zhu, K. Crozier, *Optica* **2015**, 2, 376; b) J. Li, Y. Yang, J. Li, Y. Zhang, Z. Zhang, H. Zhao, F. Li, T. Tang, H. Dai, J. Yao, *Advanced Theory and Simulations* **2020**, 3, 1900183.

[9] a) Y. Yang, W. Wang, P. Moitra, I. I. Kravchenko, D. P. Briggs, J. Valentine, *Nano letters* **2014**, 14, 1394; b) X. Zhang, Z. Tian, W. Yue, J. Gu, S. Zhang, J. Han, W. Zhang, *Advanced Materials* **2013**, 25, 4567.

[10] a) G. Zheng, H. Mühlenbernd, M. Kenney, G. Li, T. Zentgraf, S. Zhang, *Nature nanotechnology* **2015**, 10, 308; b) S. Sun, K.-Y. Yang, C.-M. Wang, T.-K. Juan, W. T. Chen, C. Y. Liao, Q. He, S. Xiao, W.-T. Kung, G.-Y. Guo, *Nano letters* **2012**, 12, 6223; c) D. Headland, E. Carrasco, S. Nirantar, W. Withayachumnankul, P. Gutruf, J. Schwarz, D. Abbott, M. Bhaskaran, S. Sriram, J. Perruisseau-Carrier, *Acs Photonics* **2016**, 3, 1019.

[11] a) C. H. Chu, M. L. Tseng, J. Chen, P. C. Wu, Y. H. Chen, H. C. Wang, T. Y. Chen, W. T. Hsieh, H. J. Wu, G. Sun, *Laser & Photonics Reviews* **2016**, 10, 986; b) Q. Wang, E. T. Rogers, B. Gholipour, C.-M. Wang, G. Yuan, J. Teng, N. I. Zheludev, *Nature Photonics* **2016**, 10, 60.

[12] J. Sautter, I. Staude, M. Decker, E. Rusak, D. N. Neshev, I. Brener, Y. S. Kivshar, *ACS nano* **2015**, 9, 4308.
[13] a) W. J. Padilla, A. J. Taylor, C. Highstrete, M. Lee, R. D. Averitt, *Physical review letters* **2006**, 96, 107401; b) M. Manjappa, Y. K. Srivastava, A. Solanki, A. Kumar, T. C. Sum, R. Singh, *Advanced materials* **2017**, 29, 1605881; c) M. Manjappa, Y. K. Srivastava, L. Cong, I. Al‐Naib, R. Singh, *Advanced Materials* **2017**, 29, 1603355; d) X. G. Zhang, Q. Yu, W. X. Jiang, Y. L. Sun, L. Bai, Q. Wang, C. W. Qiu, T. J. Cui, *Advanced science* **2020**, 7, 1903382.
[14] a) W. Y. Kim, H.-D. Kim, T.-T. Kim, H.-S. Park, K. Lee, H. J. Choi, S. H. Lee, J. Son, N. Park, B. Min, *Nature communications* **2016**, 7, 1; b) L. Ju, B. Geng, J. Horng, C. Girit, M. Martin, Z. Hao, H. A. Bechtel, X. Liang, A. Zettl, Y. R. Shen, *Nature nanotechnology* **2011**, 6, 630; c) Y. K. Srivastava, A. Chaturvedi, M. Manjappa, A. Kumar, G. Dayal, C. Kloc, R. Singh, *Advanced Optical Materials* **2017**, 5, 1700762.
[15] a) R. Singh, J. Xiong, A. K. Azad, H. Yang, S. A. Trugman, Q. Jia, A. J. Taylor, H.-T. Chen, *Nanophotonics* **2012**, 1, 117; b) B. Jin, C. Zhang, S. Engelbrecht, A. Pimenov, J. Wu, Q. Xu, C. Cao, J. Chen, W. Xu, L. Kang, *Optics express* **2010**, 18, 17504; c) Y. K. Srivastava, M. Manjappa, L. Cong, H. N. Krishnamoorthy, V. Savinov, P. Pitchappa, R. Singh, *Advanced materials* **2018**, 30, 1801257.
[16] L. Yan, W. Zhu, M. F. Karim, H. Cai, A. Y. Gu, Z. Shen, P. H. J. Chong, D. P. Tsai, D. L. Kwong, C. W. Qiu, *Advanced Optical Materials* **2018**, 6, 1800728.
[17] X. G. Zhang, W. X. Jiang, H. L. Jiang, Q. Wang, H. W. Tian, L. Bai, Z. J. Luo, S. Sun, Y. Luo, C.-W. Qiu, *Nature Electronics* **2020**, 3, 165.
[18] a) T. Driscoll, H.-T. Kim, B.-G. Chae, B.-J. Kim, Y.-W. Lee, N. M. Jokerst, S. Palit, D. R. Smith, M. Di Ventra, D. N. Basov, *Science* **2009**, 325, 1518; b) M. Liu, H. Y. Hwang, H. Tao, A. C. Strikwerda, K. Fan, G. R. Keiser, A. J. Sternbach, K. G. West, S. Kittiwatanakul, J. Lu, *Nature* **2012**, 487, 345; c) Y. Zhao, Y. Zhang, Q. Shi, S. Liang, W. Huang, W. Kou, Z. Yang, *ACS Photonics* **2018**, 5, 3040; d) C. H. Kodama, R. A. Coutu Jr, *Applied Physics Letters* **2016**, 108, 231901.
[19] a) D. Wang, L. Zhang, Y. Gu, M. Mehmood, Y. Gong, A. Srivastava, L. Jian, T. Venkatesan, C.-W. Qiu, M. Hong, *Scientific reports* **2015**, 5, 1; b) D. Wang, L. Zhang, Y. Gong, L. Jian, T. Venkatesan, C.-W. Qiu, M. Hong, *IEEE Photonics Journal* **2016**, 8, 1; c) C. Lan, H. Ma, M. Wang, Z. Gao, K. Liu, K. Bi, J. Zhou, X. Xin, *ACS applied materials & interfaces* **2019**, 11, 14229.
[20] a) Y. G. Jeong, Y. M. Bahk, D. S. Kim, *Advanced Optical Materials* **2020**, 8, 1900548; b) A. Leitis, A. Heßler, S. Wahl, M. Wuttig, T. Taubner, A. Tittl, H. Altug, *Advanced Functional Materials* **2020**, 30, 1910259.
[21] P. Pitchappa, A. Kumar, S. Prakash, H. Jani, T. Venkatesan, R. Singh, *Advanced Materials* **2019**, 31, 1808157.
[22] J. L. Valdes, L. Huitema, E. Arnaud, D. Passerieux, A. Crunteanu, *IEEE Open Journal of Antennas and Propagation* **2020**, 1, 224.
[23] a) M. Pinaud, G. Humbert, S. Engelbrecht, L. Merlat, B. Fischer, A. Crunteanu, presented at 2019 44th International Conference on Infrared, Millimeter, and Terahertz Waves (IRMMW-THz) **2019**; b) X. Fu, F. Yang, C. Liu, X. Wu, T. J. Cui, *Advanced Optical Materials* **2020**, 8, 1900628.
[24] M. Terao, T. Morikawa, T. Ohta, *Japanese Journal of Applied Physics* **2009**, 48, 080001.
[25] a) S. R. Ovshinsky, *Physical Review Letters* **1968**, 21, 1450; b) N. Yamada, E. Ohno, N. Akahira, K. i. Nishiuchi, K. i. Nagata, M. Takao, *Japanese Journal of Applied Physics* **1987**, 26, 61.
[26] C. A. Balanis, *Inc, Publication* **2005**.